

Universal Multi-Source Domain Adaptation

Yueming Yin, Zhen Yang, *Senior Member, IEEE*, Haifeng Hu, and Xiaofu Wu

Unsupervised domain adaptation enables intelligent models to transfer knowledge from a labeled source domain to a similar but unlabeled target domain. Recent study reveals that knowledge can be transferred from one source domain to another unknown target domain, called Universal Domain Adaptation (UDA). However, in the real-world application, there are often more than one source domain to be exploited for domain adaptation. In this paper, we formally propose a more general domain adaptation setting, universal multi-source domain adaptation (UMDA), where the label sets of multiple source domains can be different and the label set of target domain is completely unknown. The main challenges in UMDA are to identify the common label set between each source domain and target domain, and to keep the model scalable as the number of source domains increases. To address these challenges, we propose a universal multi-source adaptation network (UMAN) to solve the domain adaptation problem without increasing the complexity of the model in various UMDA settings. In UMAN, we estimate the reliability of each known class in the common label set via the prediction margin, which helps adversarial training to better align the distributions of multiple source domains and target domain in the common label set. Moreover, the theoretical guarantee for UMAN is also provided. Massive experimental results show that existing UDA and multi-source DA (MDA) methods cannot be directly applied to UMDA and the proposed UMAN achieves the state-of-the-art performance in various UMDA settings.

Index Terms—Universal domain adaptation, multi-source domain adaptation, universal multi-source domain adaptation, universal multi-source adaptation network, prediction margin.

I. INTRODUCTION

IN the past years, the development of deep learning greatly promotes the research on supervised image classification [1]–[7]. At present, many large-scale image classification datasets are publicly available, and deep learning models performs very well in many scenarios. However, large-scale image annotation is time-consuming and even prohibitive. This requires that deep learning models trained on the labeled dataset can generalize to unseen but similar unlabeled data. If unlabeled data and labeled data have different characteristics independent of label, they have been sampled from two different domains [8]. Therefore, domain adaptation (DA) aims to mitigate the impact of the domain gap during the process of knowledge transfer. A very challenging setting is unsupervised

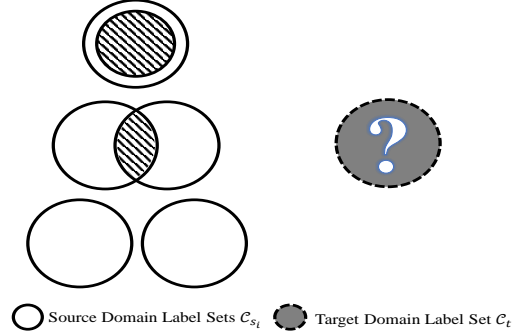


Fig. 1: Universal Multi-Source Domain Adaptation.

DA, where the source domain is fully labeled and the target domain is unlabeled. This kind of domain gap brings great challenge for the DA methods to transfer knowledge from source domain to target domain.

Depending on whether the label set of the target domain is known, existing unsupervised DA methods fall into two types: non-universal DA and universal DA [9]–[12]. And non-universal DA methods generally include closed set DA [13]–[34], partial DA [35]–[37] and open set DA [38]–[40]. These non-universal DA settings suppose that all label sets of source and target domains are known in advance, which is relatively simple to deal with. Recently, the universal DA has been receiving more attention due to the fact that the label set of target domain is completely unknown. However, existing universal DA methods [9]–[12] focus on single-source scenarios and cannot be directly applied to multi-source scenarios. For example, we have a source domain with label set A and another source domain with label set B, and these two label sets A and B are different. If we want to train a classifier to identify samples of the target domain belonging to the label set A and B, the better way is to pre-train the classifier on both of these two source domains. However, in the combined dataset, domain gap exists within the multiple distinct source domains. Unlike single-source DA [22], the same source distribution assumption doesn't hold in the case of multiple source domains. To this end, we propose a more general setting of DA as shown in Fig. 1, called universal multi-source domain adaptation (UMDA). In this setting, multiple source domains are available and the label set of target domain is completely unknown. The label set of source domains is known but the relationship between any two source label sets might be contained, intersected, or even disjoint. Therefore, more knowledge is expected to be transferred from multiple source domains to the target domain, and the classifier trained on multiple source domains can be capable of identifying more classes in the target domain.

The authors are with Nanjing University of Posts and Telecommunications, Nanjing 210003, China.

Zhen Yang is with Key Lab of Broadband Wireless Communication and Sensor Network Technology, Ministry of Education, Nanjing University of Posts and Telecommunications, Nanjing 210003, China.

Haifeng Hu and Xiaofu Wu are with National Engineering Research Center of Communications and Networking, Nanjing University of Posts and Telecommunications, Nanjing 210003, China.

Corresponding author: Yueming Yin (email: 1018010514@njupt.edu.cn) and Zhen Yang (email: yangz@njupt.edu.cn).

Differing from universal single-source domain adaptation [9] (USDA), UMDA poses two new challenges. First, in order to identify a known class in the target domain, we have to consider the domain discrepancy not only between each source domain and target domain, but also between any two distinct source domains. Second, as the number of source domains increases, the relationship between label sets of source and target domains becomes more complex. Some multi-source adaptation methods [41]–[49] have been proposed. However, these methods cannot provide the promising performance in the target domain. Furthermore, with the increase of the number of source domains, the model complexity of these methods makes it difficult to implement in an efficient way.

To tackle these two challenges, we design a Universal Multi-Source Adaptation Network (UMAN) with a novel weighting mechanism to identify the common classes of source and target domains, which mitigates the domain gaps between a large number of source domains and an unknown target domain without increasing the complexity of the model. Specifically, we first introduce the *margin vector* to UMDA, which defined as the empirical prediction margin with respect to each pseudo-label as shown in Fig. 2. Prediction margin measures the confidence in assigning a target sample to its pseudo-label. Therefore, a pseudo-label with a larger prediction margin is more likely to be a common class between source and target domains. It can be seen that we can accurately identify the common label set by using margin vector related operations. In UMAN, we also design a joint cross-entropy loss and a joint adversarial loss to align not only the distributions between the source domains but also between the source and target domains in their common label set. Note that in the joint adversarial loss, each class in different source domains is weighted by the same *margin vector*, so the complexity of UMAN become insensitive to the number of source domains.

Moreover, we provide theoretical analysis of the two joint losses in UMAN, and obtain two theoretical guarantees. First, optimizing the joint cross-entropy loss is equivalent to aligning the distribution of source domains in their common label set. Second, optimizing the joint adversarial loss is equivalent to aligning the distribution between the center of multiple source domains and target domain in their common label set.

The main contributions of this paper can be summarized as:

- 1) We propose a more practical Universal Multi-Source Domain Adaptation (UMDA) setting, where the label sets of multiple source domains can be different and the label set of target domain is completely unknown. Thus, the knowledge of multiple source domains can be transferred to target domain in an unsupervised way.
- 2) We propose a Universal Multi-Source Adaptation Network (UMAN) with a novel margin vector for UMDA. The common label set can be identified via the margin vector, which helps adversarial training to better align the distributions of multiple source domains and target domain in an efficient way, and does not incur extra model complexity in various UMDA settings. Moreover, we make theoretical analysis of the two losses of UMAN, which provides the theoretical guarantees for

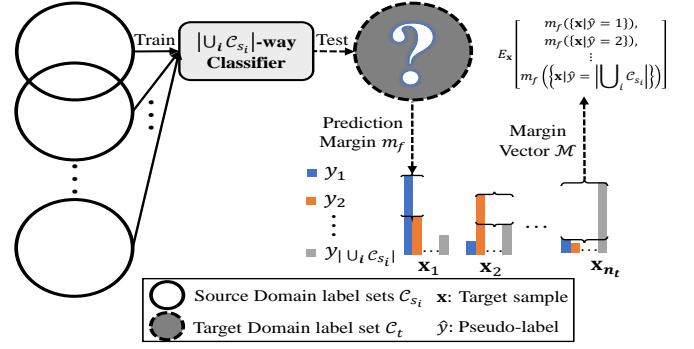


Fig. 2: An illustration of margin vector. We employ the prediction margin as the reliability of pseudo-label in the common label set.

alignment of distribution of source and target domains in the common label set.

- 3) Massive experimental results show that the proposed UMAN works stably across various UMDA settings and outperforms the state-of-the-art methods by large margins.

II. RELATED WORK

We briefly review recent domain adaptation methods in this section. According to the number of source domains, these methods fall into two categories: single-source domain adaptation and multi-source domain adaptation. In single-source domain adaptation, according to the constraint on the relationship between source and target label sets, methods are divided into closed set domain adaptation, partial domain adaptation, open set domain adaptation and universal domain adaptation. In multi-source domain adaptation, existing methods primarily focus on closed set setting.

A. Single-Source Domain Adaptation

Closed Set Single-Source Domain Adaptation. Closed set single-source domain adaptation focuses on mitigating the impact of the domain gap between source and target domains. Closed set single-source domain adaptation methods mainly contain two categories: feature adaptation and generative model. Feature adaptation methods [13]–[21], [31], [34] diminish the feature distribution discrepancy between source and target domains by minimizing statistical distances, such as \mathcal{H} -divergence [22], $\mathcal{H}\Delta\mathcal{H}$ -divergence [50] and MMD [14], [32]. Methods based on generative models [23]–[30], [33] synthesize target samples as data augmentation and match domains in pixel or feature levels.

Partial Single-Source Domain Adaptation. Partial single-source domain adaptation (PSDA) [35]–[37] transfers a learner from a big source domain to a small target domain, where the source label set contains the target label set. To solve PSDA, Cao *et al.* [35] utilized multiple domain discriminators with class-level and instance-level weighting mechanism to perform per-class adversarial distribution matching. Zhang *et al.* [36] constructed an auxiliary domain discriminator to estimate the probability of a source sample being similar to the target domain. Cao *et al.* [37] further improved PSDA by

employing an adversarial network and jointly applying class-level weighting on the source classifier.

Open Set Single-Source Domain Adaptation. Busto *et al.* [38] first proposed open set single-source domain adaptation (OSSDA). The classes private to both domains are recognized as an “unknown” class. They use an Assign-and-Transform-Iteratively (ATI) algorithm to map target samples to source classes and then train SVMs for final classification. Saito *et al.* [39] modified OSSDA by requiring no data of the source private label set and extends the source classifier by adding an “unknown” class and trains it adversarially among classes. Recently, Luo *et al.* [40] addressed conditional shift by constructing graph neural networks for OSSDA.

Universal Single-Source Domain Adaptation. For these aforementioned single-source DA methods, prior knowledge about label sets is assumed to be known. You *et al.* [9] first proposed universal single-source domain adaptation (USDA), which requires no prior knowledge on the label sets. In [9], a novel criterion was proposed to quantify the transferability of each sample and weight samples during domain adversarial training. Recently, Lifshitz *et al.* [10] adopted a sample selection approach to promote the performance for USDA. Saito *et al.* [11] solved USDA problem through self-supervision. Kundu *et al.* [12] proposed a source-free USDA method for real-time adaptation.

B. Closed Set Multi-Source Domain Adaptation

Existing methods for multi-source domain adaptation primarily focus on a relatively simple application scenario. That is, the target data is unlabeled but available during the training process, the source data is fully labeled, the source and target data are observed in the same data space, and the label sets of all sources and the target are the same [51]. Here, we call these methods as closed set multi-source domain adaptation (CSMDA). The idea behind CSMDA is based on the seminal theoretical model [22], [50]. Mansour *et al.* [52] assumed that the target distribution can be approximated by a mixture of the multiple source distributions. Therefore, weighted combination of source classifiers has been widely employed for CSMDA. Moreover, tighter cross domain generalization bound and more accurate measurements on domain discrepancy can provide intuitions to derive effective CSMDA algorithms. Hoffman *et al.* [53] derived a novel bound using DC-programming and calculated more accurate combination weights. Zhao *et al.* [42] extended the generalization bound of seminal theoretical model to multiple sources under both classification and regression settings. Besides the domain discrepancy between the target and each source [42], [53], Li *et al.* [54] also considered the relationship between pairwise sources and derived a tighter bound on weighted multi-source discrepancy.

In closed set multi-source domain adaptation, category shift was first formally considered in [41], where each source domain may not contain all the classes in the target domain. However, the union of all source label sets is the same as target label set, which can be still categorized as closed set multi-source domain adaptation.

III. OUR APPROACH

In this section, we introduce the scenario of Universal Multi-Source Domain Adaptation (UMDA) and then propose a novel Universal Multi-Source Adaptation Network (UMAN) for this scenario.

A. Problem Setting

In Universal Multi-Source Domain Adaptation, M source domains $\mathcal{D}_{s_i} = \{(\mathbf{x}_j^{s_i}, y_j^{s_i})\}, i = 1, 2, \dots, M$ consisting of n_{s_i} labeled samples and a target domain $\mathcal{D}_t = \{(\mathbf{x}_k^t)\}$ of n_t unlabeled samples are provided at training. Note that the source data are sampled from distribution p_i while the target data from distribution q . We use \mathcal{C}_{s_i} to denote the label set of source domain \mathcal{D}_{s_i} and \mathcal{C}_t the label set of target domain. $\mathcal{C}_i = \mathcal{C}_{s_i} \cap \mathcal{C}_t$ is the common label set shared by \mathcal{D}_{s_i} and \mathcal{D}_t . $\bar{\mathcal{C}}_{s_i} = \mathcal{C}_{s_i} \setminus \mathcal{C}_i$ and $\bar{\mathcal{C}}_t = \mathcal{C}_t \setminus \{\bigcup_i \mathcal{C}_i\}$ represent the label set private to the source domain \mathcal{D}_{s_i} and the target domain \mathcal{D}_t respectively. And $\mathcal{C}_s = \bigcup_i \mathcal{C}_{s_i}$ is the label set which contains all the known labels in source domains, $\mathcal{C} = \bigcup_i \mathcal{C}_i$ is the union of common label sets between each source domain and the target domain, and $\bar{\mathcal{C}}_s = \bigcup_i \bar{\mathcal{C}}_{s_i}$ is the common label set between source domains that does not appear in target domain. $p_{\mathcal{C}_i}$ and $p_{\bar{\mathcal{C}}_{s_i}}$ are used to denote the distribution of source data with labels in the label set \mathcal{C}_i and $\bar{\mathcal{C}}_{s_i}$ respectively, and $q_{\mathcal{C}}, q_{\mathcal{C}_i}, q_{\bar{\mathcal{C}}_t}$ for target distributions with labels in the label set $\mathcal{C}, \mathcal{C}_i, \bar{\mathcal{C}}_t$ respectively. Note that the target data are fully unlabeled, and the target label sets (inaccessible at training) are only used for defining the UMDA problem.

The definition of commonness between two domains introduced in [9] is the Jaccard distance of two label sets: $\xi = \frac{|\mathcal{C}_s \cap \mathcal{C}_t|}{|\mathcal{C}_s \cup \mathcal{C}_t|}$. Closed set domain adaptation is a special case of universal domain adaptation when $\xi = 1$. In UMDA, Jaccard distance is modified as $\xi_i = \frac{|\mathcal{C}_{s_i} \cap \mathcal{C}_t|}{|\mathcal{C}_{s_i} \cup \mathcal{C}_t|}$ associated with the i -th source domain and the target domain. Similarly, $\xi_{ij} = \frac{|\mathcal{C}_{s_i} \cap \mathcal{C}_{s_j}|}{|\mathcal{C}_{s_i} \cup \mathcal{C}_{s_j}|}$ is defined as Jaccard distance between source label sets. Both domain gaps and category gaps exist in UMDA setting. In other words, domain gaps exist not only between each source domain and target domain but also between any two source domains, i.e. $p_{\mathcal{C}_i} \neq q_{\mathcal{C}_i}$ and $p_i \neq p_j$. The main task for UDA is to mitigate the impact of $p_{\mathcal{C}_i} \neq q_{\mathcal{C}_i}$. Meanwhile, the learning model should distinguish between target samples coming from known classes in \mathcal{C} and unknown classes in $\bar{\mathcal{C}}_t$. Finally, the model should be learned to minimize the target risk in $\mathcal{C} = \bigcup_i \mathcal{C}_i$, i.e. $\min \mathbb{E}_{(\mathbf{x}, y) \sim q_{\mathcal{C}}} [f(\mathbf{x}) \neq y]$.

B. Margin Vector

We first introduce a class-wise weighting mechanism guaranteed by margin theory to UMDA. The margin between features and the classification surface makes an important impact on designing generalizable classifier. Therefore, a margin theory for classification was developed by [55] and [56], where the 0-1 loss for classification is replaced by the marginal loss. Differ from [55] and [56], the prediction margin in this paper is to quantify the probability of a target label belonging to the common label set. In particular, we define the *margin* of

a hypothesis predictor (a $|\mathcal{C}_s|$ -way classifier) f at a pseudo-labeled example \mathbf{x} of target domain as

$$m_f(\mathbf{x}) \triangleq f(\mathbf{x}, \hat{y}) - \max_{y \neq \hat{y}} f(\mathbf{x}, y), \quad (1)$$

$$\hat{y} \triangleq \arg \max_{y \in [1, |\mathcal{C}_s|]} f(\mathbf{x}, y), \quad (2)$$

where $f(\mathbf{x}, y)$ is the classification probability of \mathbf{x} belonging to the y -th class, and \hat{y} is the pseudo-label of \mathbf{x} . This *margin* measures the confidence in assigning an example to its pseudo-label. In particular, wrong pseudo-labeled samples and samples of unknown classes will have a small margin, where the classification surface intersects here. If $m_f(\mathbf{x}) = 1$, \mathbf{x} is considered most likely to come from known classes. Similarly, if $m_f(\mathbf{x}) = 0$, \mathbf{x} is most likely to come from unknown classes.

Then, the empirical *margin vector* over a data distribution \mathcal{D} is defined as

$$\mathcal{M}(\mathcal{D}, f) \triangleq \mathbb{E}_{\mathbf{x} \in \mathcal{D}} [m_f(\{\mathbf{x}|\hat{y} = 1\}), \dots, m_f(\{\mathbf{x}|\hat{y} = |\mathcal{C}_s|\})]^T. \quad (3)$$

In this definition, the i -th dimension of the *margin vector* is the empirical *margin* of samples with the i -th pseudo-label. In UMDA, *margin vector* can be used to calculate over the classifier trained on each source domain or the classifier trained on the integrated source domains, which obtains the reliability of each source classes belonging to the common label set \mathcal{C}_i or $\mathcal{C} = \bigcup_i \mathcal{C}_i$ respectively.

C. Target Margin Register and Transferability Criterion

We first introduce a target margin register (TMR) to UMDA. The TMR is formulated as a \mathcal{C}_s -dimensional vector \mathbf{V}_{TMR} , which is updated in each training step. The updated rule is defined as

$$\mathbf{V}_{TMR}^{t+1} = \frac{1}{t+1} (t \times \mathbf{V}_{TMR}^t + \mathcal{M}(\mathcal{D}_t^b, f)), \quad (4)$$

$$\mathbf{V}_{TMR}^0 = \underbrace{[0, 0, \dots, 0]^T}_{|\mathcal{C}_s|}, \quad (5)$$

where $\mathcal{M}(\mathcal{D}_t^b, f)$ is the *margin vector*, defined in Eq. 3, which outputs a \mathcal{C}_s -dimensional *margin vector* over \mathcal{D}_t^b and f , \mathcal{D}_t^b denotes a batch of target samples from \mathcal{D}_t , f denotes the prediction function of the classifier. Note that $t \times \mathbf{V}_{TMR}^t$ is the accumulated *margin vector* of previous t steps, t is the updating step and $t < T$, where T is the maximum step number for training. \mathbf{V}_{TMR}^t denotes the TMR-vector at step t . In Eq. 4, the first term is equal to the accumulated *margin vector* in the previous steps, the second term is the *margin vector* of \mathcal{D}_t^b and f in the current training step. The definition of TMR is to calculate the average of the *margin vector* corresponding to all batches of target samples during training.

Each dimension of \mathbf{V}_{TMR} represents the empirical prediction margin, which means the level of reliability that the corresponding label in the source domain belonging to the label set of the target domain. Therefore, this margin can be

directly used to weight a source sample $\mathbf{x}_j \in \mathcal{D}_s$ by its labels y_j :

$$w^s(y_j) = \mathbf{V}_{TMR}[y_j], \quad (6)$$

where $w^s(y_j)$ indicates the probability of the source label y_j belonging to the common label set \mathcal{C} , and $\mathbf{V}_{TMR}[y_j]$ is the dimension of \mathbf{V}_{TMR} corresponding to y_j . Note that in Eq. 6, TMR-vector, shared by all source domains, has $|\mathcal{C}_s|$ components associated with all the known labels in source domains. Each class in different source domains is weighted by the same TMR-vector, so the complexity of UMAN become insensitive to the number of source domains.

In the same way, *margin vector* is utilized to weight target samples with respect to their pseudo-labels. Considering the confidence in assigning a target sample to its pseudo-label varies between target samples, the ultimate probability of each target sample \mathbf{x}_k belonging to the union of common label sets $\mathcal{C} = \bigcup_i \mathcal{C}_i$ is defined by both class-wise and sample-wise reliabilities:

$$w^t(\mathbf{x}_k, f) = m_f(\mathbf{x}_k) \cdot \mathbf{V}_{TMR}[\hat{y}_k], \quad (7)$$

where $m_f(\mathbf{x}_k)$ is the *margin* of a target sample \mathbf{x}_k calculated by the classifier f trained on the source domains in Eq. 1. $\mathbf{V}_{TMR}[\hat{y}_k]$ is the dimension of \mathbf{V}_{TMR} corresponding to \hat{y}_k , and \hat{y}_k is the pseudo label of \mathbf{x}_k defined in Eq. 2.

Unlike [9], we define the weighting mechanism in terms of class rather than individual sample in the source domain, and consider both class-wise weights and sample-wise reliabilities in the target domain. **Essentially**, for all source domains, samples in the same class should share a common weight, when the probability of a class belonging to \mathcal{C} can be estimated. And the weight of classes in the common label set should be consistent through all the domains. Note that $w^s(y_j)$ (or $w^t(\mathbf{x}_k, f)$) is further normalized as [9].

D. Universal Multi-Source Adaptation Network

The main challenge of UMDA is to mitigate the impact of $p_{\mathcal{C}_i} \neq q_{\mathcal{C}_i}$. Unlike [41], [57]–[61], we use a shared feature extractor, a shared classifier and a shared discriminator to solve UMDA problem. This means the proposed UMAN can work on a large number of source domains without increasing complexity. To this end, let $F: \mathbb{R}^{l \times w} \rightarrow \mathbb{R}^d$ be the feature extractor, and $G: \mathbb{R}^d \rightarrow \{0, 1, \dots, |\mathcal{C}_s| - 1\}$ be the classifier. Here, $l \times w$ and d denote the dimension of input samples and feature representations respectively. Input \mathbf{x} from multiple domains are forwarded into F to obtain the feature $\mathbf{z} = F(\mathbf{x})$, then, \mathbf{z} is L2-normalized and fed into G to estimate the classification probability $G^c(\mathbf{z})$ of \mathbf{x} over the c -th class in \mathcal{C}_s . The probabilities of source input \mathbf{x}_i are reserved to calculate the joint cross-entropy loss E_G with labels in all source domains:

$$E_G = \frac{1}{M} \sum_{i=1}^M \mathbb{E}_{(\mathbf{x}, y) \sim p_i} L(y, G(F(\mathbf{x}))), \quad (8)$$

where $L(\cdot, \cdot)$ denotes the cross-entropy loss, $F(\mathbf{x})$ is the L2-normalized feature. The optimization on Eq. 8 is equivalent to aligning the distributions between any two source domains in

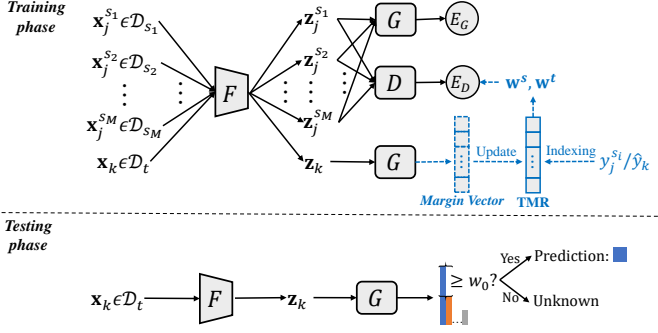


Fig. 3: The training and testing phases of proposed UMAN.

their common label sets, which is guaranteed by Theorem 1 (see below).

Let $D : \mathbb{R}^d \rightarrow \{0, 1\}$ be the binary classifier discriminating input feature \mathbf{z} from the source domain or the target domain. Inspired by [9], the domain classifier D can be trained by weighting $w^s(y_j)$ defined in Eq. 6 and $w^t(\mathbf{x}_k, G \circ F)$ defined in Eq. 7 as

$$E_D = -\frac{1}{M} \sum_{i=1}^M \mathbb{E}_{(\mathbf{x}, y) \sim p_i} w^s(y) \log D(F(\mathbf{x})) - \mathbb{E}_{\mathbf{x} \sim q} w^t(\mathbf{x}, G \circ F) \log (1 - D(F(\mathbf{x}))), \quad (9)$$

where $G \circ F$ is the entity of the classifier f in Eq. 7, and M is the number of source domains. Through the above adversarial learning, the center of the distributions of source domains and the distribution of target domain are aligned in \mathcal{C} as precisely as possible, which is guaranteed by Theorem 2. Note that the distributions between any two source domains in their common label set are aligned according to Theorem 1. Therefore, all distributions of source and target domains match each other well in the common label set.

Optimization. The whole training procedure can be written as:

$$\max_D \min_{F, G} E_G - E_D. \quad (10)$$

This optimization objective is very simple but effective. We use the gradient reversal layer [15] to reverse the gradient between F and D , this allows the optimization of all modules in an end-to-end way. Note that both E_G and E_D calculate expectations on multiple source domains. Even if multiple source domains are merged into a mixed source domain, UMAN still works. This means that UMAN can complete the domain adaptation process in the case of the domain gap among multiple source domains.

Inference. Finally, a target test sample \mathbf{x} is assigned to either corresponding known class of the source domains or the unknown class:

$$y(\mathbf{x}) = \begin{cases} \arg \max_{c \in \mathcal{C}_s} G^c(F(\mathbf{x})), & m_{G \circ F}(\mathbf{x}) \geq w_0 \\ \text{unknown}, & \text{otherwise} \end{cases} \quad (11)$$

where $m_{G \circ F}(\mathbf{x})$ is the *margin* of the test sample \mathbf{x} calculated by the entity of classifier $G \circ F$ according to Eq. 1, w_0 is the threshold for separating unknown-class samples from known-class samples. The whole model is shown in Fig. 3, the algorithm of UMAN is shown in Algorithm 1, and the

theoretical guarantees of UMAN are provided in Section III-E. Note that in UMAN algorithm, we update V_{TMR} only when the max source error lower than a threshold ϵ .

Algorithm 1: UMAN Algorithm

Input: T : max iteration;

w_0 : the threshold for separating unknown-class samples from known-class samples;

$\mathcal{D}_{s_i} = \{\mathbf{x}_j^{s_i}, y_j^{s_i}\}_{j=1}^{n_{s_i}}, i = 1, 2, \dots, M$: source training datasets;

$\mathcal{D}_t = \{\mathbf{x}_k\}_{k=1}^{n_t}$: target training dataset;

F : pretrained feature extractor parameterized by θ_f ;

G : randomly initialized classifier parameterized by θ_g ;

D : randomly initialized domain classifier parameterized by θ_d ;

Output: θ_f, θ_g and θ_d .

1 Training:

2 set $t = 0, \epsilon = 0.1$ and initialize $V_{TMR} = V_{TMR}^0$;

3 **while** $t < T$ **do**

4 **for each batch** $(\mathcal{D}_{s_1}^b, \mathcal{D}_{s_2}^b, \dots, \mathcal{D}_{s_M}^b, \mathcal{D}_t^b)$ **in** $(\mathcal{D}_{s_1}, \mathcal{D}_{s_2}, \dots, \mathcal{D}_{s_M}, \mathcal{D}_t)$ **do**

5 obtain extracted features on each domain:

6 $\mathbf{z}_j^{s_i} = F(\mathbf{x}_j^{s_i})$ and $\mathbf{z}_k = F(\mathbf{x}_k)$;

7 obtain classification results using softmax:

8 $G(\mathbf{z}_j^{s_i})$ and $G(\mathbf{z}_k)$;

9 calculate the margin $m_{G \circ F}(\mathbf{x}_k)$ by Eq. 1 and 2;

10 obtain the *margin vector* $\mathcal{M}(\mathcal{D}_t^b, F \circ G)$ by Eq. 3;

11 calculate source error ($\mathbf{1}\{\cdot\} = 1$ if $\{\cdot\}$ is true):

12 $error(\mathcal{D}_{s_i}) = \frac{1}{n_{s_i}} \sum_{j=1}^{n_{s_i}} \mathbf{1}\{G(F(\mathbf{x}_j)) \neq y_j\}$;

13 **if** $\max_i error(\mathcal{D}_{s_i}) < \epsilon$ **then**

14 | update TMR by Eq. 4 and 5;

15 **end**

16 weight $\mathbf{x}_j^{s_i}$ using TMR-vector by Eq. 6;

17 weight \mathbf{x}_k using TMR-vector and *margin* by Eq. 7;

18 calculate E_G by Eq. 8 and E_D by Eq. 9;

19 update θ_f, θ_g and θ_d by optimizing Eq. 10

20 using statistical gradient descent;

21 let $t \leftarrow t + 1$;

22 **end**

23 **end**

24 **Testing:**

25 Test data \mathbf{x} is forwarded to obtain $G^c(F(\mathbf{x}))$ over $c \in \mathcal{C}_s$;

26 **if** $m_{G \circ F}(\mathbf{x}) \geq w_0$ **then**

27 | label \mathbf{x} with $y = \arg \max_c G^c(F(\mathbf{x}))$;

28 **else**

29 | reject \mathbf{x} as an unknown class;

30 **end**

E. Theoretical Guarantees of UMAN

In this section, we provide theoretical analysis of the proposed UMAN and show how it works. As shown in Eq. 10, the objective function of UMAN consists of two parts: E_G

and E_D . For samples drawn from M source domains, UMAN employs the same category classifier C and domain classifier D , we have the following theorems:

Theorem 1. Let p_{ij} be the distribution of the i -th source domain with labels in the label set $\mathcal{C}_{s_i} \cap \mathcal{C}_{s_j}$, \bar{p}_i be the distribution of the i -th source domain in the private label set. Let G' be an auxiliary classifier with the same structure as G . Minimize E_G with respect to F and G is equivalent to

$$\begin{aligned} \max_{G'} \min_{F, G} & -\frac{1}{M} \sum_{i=1}^{M-1} \sum_{j=i+1}^M \mathbb{E}_{(\mathbf{x}, y) \sim p_{ij}} \log G'^y(F(\mathbf{x})) \\ & - \mathbb{E}_{(\mathbf{x}, y) \sim p_{ji}} \log(1 - G'^y(F(\mathbf{x}))) \\ & - \frac{1}{M} \sum_{i=1}^M \mathbb{E}_{(\mathbf{x}, y) \sim \bar{p}_i} \log G^y(F(\mathbf{x})). \end{aligned} \quad (12)$$

Proof. For simplicity, we only prove Theorem 1 when the label sets of every two source domains are disjoint. If they intersect, Theorem 1 can also be proved similarly. We divide E_G , defined in Eq. 8, into three parts:

$$\begin{aligned} E_G = & -\frac{1}{M} \sum_{i=1}^{M-1} \sum_{j=i+1}^M \mathbb{E}_{(\mathbf{x}, y) \sim p_{ij}} \log G^y(F(\mathbf{x})) \\ & - \mathbb{E}_{(\mathbf{x}, y) \sim p_{ji}} \log G^y(F(\mathbf{x})) \\ & - \frac{1}{M} \sum_{i=1}^M \mathbb{E}_{(\mathbf{x}, y) \sim \bar{p}_i} \log G^y(F(\mathbf{x})). \end{aligned} \quad (13)$$

The gradients of the first two parts have the same direction when minimizing E_G for G and F . And the optimal solution for both two parts is

$$(G \circ F)^*(x) = \{G \circ F | \forall (\mathbf{x}, y) \sim p_{ij}, G^y(F(\mathbf{x})) = 1\}, \quad (14)$$

for all $i, j = 1, \dots, M$ and $i \neq j$. When $G \circ F = (G \circ F)^*$, the distributions of $F(\mathbf{x} \sim p_{ij})$ and $F(\mathbf{x} \sim p_{ji})$ are forced to be indistinguishable for G . Therefore, the first two parts of Eq. 13 can be taken as an equivalent objective for F :

$$\begin{aligned} \max_{G'} \min_F & -\frac{1}{M} \sum_{i=1}^{M-1} \sum_{j=i+1}^M \mathbb{E}_{(\mathbf{x}, y) \sim p_{ij}} \log G'^y(F(\mathbf{x})) \\ & - \mathbb{E}_{(\mathbf{x}, y) \sim p_{ji}} \log(1 - G'^y(F(\mathbf{x}))). \end{aligned} \quad (15)$$

Here, G' plays a role of a discriminator to force F to extract indistinguishable features of samples drawn from p_{ij} and p_{ji} . Hence, the distributions of any two source domains are aligned in their common label set. \square

Theorem 2. The max-min of E_D with respect to D and F is equivalent to minimizing the Jensen-Shannon Divergence between the center of the distributions of source domains $\mathcal{D}_{s_i} = \{(\mathbf{x}_j^{s_i}, y_j^{s_i})\}, i = 1, 2, \dots, M$ and the distribution of target domain $\mathcal{D}_t = \{(\mathbf{x}_k^t)\}$ in the union common label set $\mathcal{C} = \bigcup_i \mathcal{C}_i$, i.e.

$$\begin{aligned} \max_D \min_F & -E_D \\ \iff \min_F & \text{JSD}(\frac{1}{M} \sum_{i=1}^M F(p_{C_i}(\mathbf{x}_j)) || F(q_C(\mathbf{x}_k))). \end{aligned} \quad (16)$$

Proof. Here, we consider that the ideal distribution of weights can be approximated by Eq. 6 and Eq. 7, i.e.,

$$w^s(y_j) \rightarrow \begin{cases} 1, & y_j \in \mathcal{C} \\ 0, & y_j \notin \mathcal{C}, \end{cases} \quad (17)$$

$$w^t(\mathbf{x}_k, f) \rightarrow \begin{cases} 1, & y_k \in \mathcal{C} \\ 0, & y_k \notin \mathcal{C}. \end{cases} \quad (18)$$

Then, E_D defined in Eq. 9 can be written as

$$\begin{aligned} E_D(F, D) \rightarrow & -\frac{1}{M} \sum_{i=1}^M \mathbb{E}_{(\mathbf{x}, y) \sim p_{C_i}} \log D(F(\mathbf{x})) \\ & - \mathbb{E}_{\mathbf{x} \sim q_C} \log(1 - D(F(\mathbf{x}))), \end{aligned} \quad (19)$$

Given $\mathbf{z} = F(x)$, we have the optimal solution when maximizing $-E_D$ for D :

$$D^*(\mathbf{z}) \rightarrow \frac{\frac{1}{M} \sum_{i=1}^M p_{C_i}(\mathbf{z})}{\frac{1}{M} \sum_{i=1}^M p_{C_i}(\mathbf{z}) + q_C(\mathbf{z})}, \quad (20)$$

where $p_{C_i}(\mathbf{z})$ and $q_C(\mathbf{z})$ are the probabilities that $\mathbf{x} = F^{-1}(\mathbf{z})$ can be sampled from p_{C_i} and q_C respectively. Optimal value can be calculated as follows:

$$\begin{aligned} -E_D(F, D^*) \rightarrow & \frac{1}{M} \sum_{i=1}^M \mathbb{E}_{(\mathbf{x}, y) \sim p_{C_i}} \frac{\frac{1}{M} \sum_{i=1}^M p_{C_i}(\mathbf{z})}{\frac{1}{M} \sum_{i=1}^M p_{C_i}(\mathbf{z}) + q_C(\mathbf{z})} \\ & + \mathbb{E}_{\mathbf{x} \sim q_C} \frac{q_C(\mathbf{z})}{\frac{1}{M} \sum_{i=1}^M p_{C_i}(\mathbf{z}) + q_C(\mathbf{z})} \\ = & \int_f \frac{1}{M} \sum_{i=1}^M p_{C_i}(\mathbf{z}) \frac{\frac{1}{M} \sum_{i=1}^M p_{C_i}(\mathbf{z})}{\frac{1}{M} \sum_{i=1}^M p_{C_i}(\mathbf{z}) + q_C(\mathbf{z})} d\mathbf{z} \\ & + \int_{\mathbf{z}} q_C(f) \frac{q_C(\mathbf{z})}{\frac{1}{M} \sum_{i=1}^M p_{C_i}(\mathbf{z}) + q_C(\mathbf{z})} d\mathbf{z} \\ = & -2 \log 2 + \int_{\mathbf{z}} \frac{1}{M} \sum_{i=1}^M p_{C_i}(f) \frac{\frac{1}{M} \sum_{i=1}^M p_{C_i}(\mathbf{z})}{\frac{1}{2M} \sum_{i=1}^M p_{C_i}(\mathbf{z}) + \frac{1}{2} q_C(\mathbf{z})} d\mathbf{z} \\ & + \int_{\mathbf{z}} q_C(f) \frac{q_C(\mathbf{z})}{\frac{1}{2M} \sum_{i=1}^M p_{C_i}(\mathbf{z}) + \frac{1}{2} q_C(\mathbf{z})} d\mathbf{z} \\ = & -2 \log 2 + \text{KL}(\frac{1}{M} \sum_{i=1}^M p_{C_i} || \frac{\frac{1}{M} \sum_{i=1}^M p_{C_i} + q_C}{2}) \\ & + \text{KL}(q_C || \frac{\frac{1}{M} \sum_{i=1}^M p_{C_i} + q_C}{2}) \\ = & -2 \log 2 + 2\text{JSD}(\frac{1}{M} \sum_{i=1}^M p_{C_i} || q_C), \end{aligned} \quad (21)$$

where $\text{KL}(\cdot || \cdot)$ is the Kullback-Leibler Divergence and $\text{JSD}(\cdot || \cdot)$ is the Jensen-Shannon Divergence. Then, with minimizing $-E_D$ for F with a much smaller learning rate, we get an equivalent optimization:

$$\min_F \text{JSD}(\frac{1}{M} \sum_{i=1}^M F(p_{C_i}(\mathbf{x}_j)) || F(q_C(\mathbf{x}_k))), \quad (22)$$

where \mathbf{x}_j are drawn from p_{C_i} and \mathbf{x}_k are drawn from q_C . Hence, the center of the distributions of source domains and the distribution of target domain are aligned in their common label set. \square

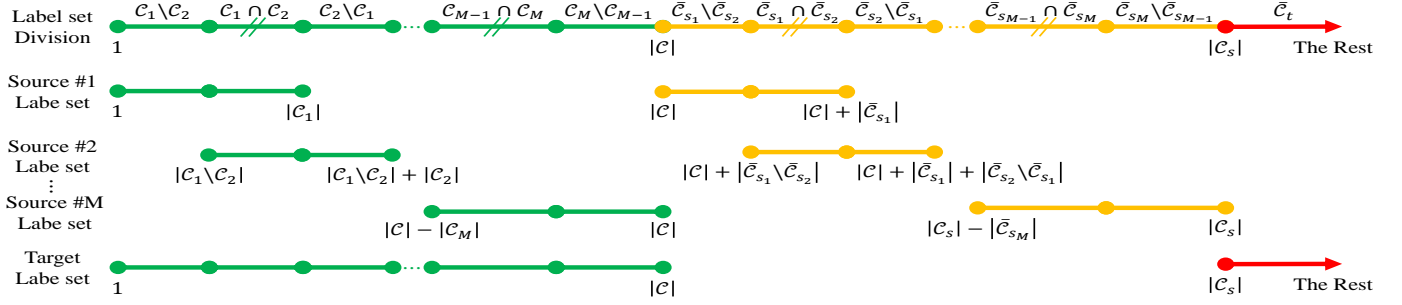


Fig. 4: The division rule of the common label set (green), the source private label set (orange) and the target private label set (red). Note that the lengths of the intersections are as equal as possible in the common label set (green double slash) and the source private label set (orange double slash) respectively.

IV. EXPERIMENTS

A. Experimental Setup

1) Label Sets

The division rule of all the label sets introduced in Section III-A is shown in Fig. 4. Each domain contains two types of label sets: common and private. Therefore, we use a matrix to describe a specific UMDA setting, called **UMDA-Matrix**, which is defined as

$$\begin{bmatrix} |C_1| & |C_2| & \cdots & |C_M| & |C| \\ |\bar{C}_{s_1}| & |\bar{C}_{s_2}| & \cdots & |\bar{C}_{s_M}| & |\bar{C}_t| \end{bmatrix}. \quad (23)$$

The first line of Eq. 23 is the size of the common label set of all the domains, and the second line the private label set. The first M columns of Eq. 23 are the label set of the source domains, and the last column the target domain. In this way, UMDA settings can be determined by the division rule and the UMDA-Matrix.

2) Datasets

The UMDA settings on each dataset are shown in Table I, where multiple UMDA-Matrices mean that multiple UMDA settings are considered in one dataset. More settings are explored in Section IV-C. The following is additional information about the datasets:

Office-31 [62] dataset contains 31 categories in 3 different domains: **A**, **D**, **W**. There are at most two source domains and one target domain, i.e. $M = 2$. We use the 10 classes shared by Office-31 and Caltech-256 [63] as the total common label set C , and the rest of the classes are sorted in alphabetical order.

Office-Home [64] is a larger dataset with 65 classes in 4 different domains: Artistic (**Ar**), Clip-Art (**Cl**), Product (**Pr**) and Real-World (**Rw**) images. In this dataset, M can be 2 and 3. All the classes are sorted in alphabetical order.

VisDA2017+ImageCLEF-DA. VisDA2017 [65] dataset focuses on a special domain adaptation setting (simulation to real). The source domain consists of simulated images (**S**) generated by game engines and target domain consists of real-world images (**R**). ImageCLEF-DA¹ is a benchmark dataset for ImageCLEF 2014 domain adaptation challenge, which is organized by selecting the common categories shared by the following three public datasets. Here, each dataset is

TABLE I: The UMDA settings on different datasets.

Datasets	classes	Domains	Images	UMDA-Matrices
Office-31	31	A	2817	$\begin{bmatrix} 7 & 7 & 10 \\ 5 & 5 & 11 \end{bmatrix}$
		D	498	
		W	795	
Office-Home	65	Ar	2427	$\begin{bmatrix} 7 & 7 & 10 \\ 5 & 5 & 50 \\ 4 & 4 & 10 \\ 2 & 2 & 50 \end{bmatrix}$
		Cl	4365	
		Pr	4439	
		Rw	4357	
VisDA2017 + ImageCLEF-DA	17	S	152397	$\begin{bmatrix} 4 & 4 & 7 \\ 1 & 1 & 3 \\ 3 & 3 & 7 \\ 1 & 1 & 2 \\ 2 & 2 & 7 \\ 1 & 1 & 1 \end{bmatrix}$
		R	55388	
		C	600	
		I	600	
		P	600	



Fig. 5: Some samples in following datasets (from top to bottom and left to right). (1) **Office-31**: Amazon (**A**), Dslr (**D**) and Webcam (**W**). (2) **Office-Home**: Artistic (**Ar**), Clip-Art (**Cl**), Product (**Pr**) and Real-World images (**W**). (3) **VisDA2017**: Synthetic (**Syn**) and Real images (**Real**). (4) **ImageCLEF-DA**: Caltech-256 (**C**), ImageNet ILSVRC 2012 (**I**), and Pascal VOC 2012 (**P**).

considered as a domain: Caltech-256 (**C**), ImageNet ILSVRC 2012 (**I**), and Pascal VOC 2012 (**P**). In this dataset, M can be 2, 3 and 4. Classes are numbered in this way: No. 1-7 classes are the shared classes of five datasets, in alphabet order, No. 8-12 classes are the remaining classes of **S** and **R**, and No. 13-17 classes are the remaining classes of **C**, **I** and **P**.

Some samples in each dataset are shown in Fig. 5.

¹<https://www.imageclef.org/2014/adaptation>

3) Evaluation Details

Compared Methods. The proposed UMAN is compared with (1) Single-source-only without domain adaptation (DA): **ResNet** [66], (2) closed set single-source DA: Domain-Adversarial Neural Networks (**DANN**) [15], Residual Transfer Networks (**RTN**) [18], (3) partial single-source DA: Importance Weighted Adversarial Nets (**IWAN**) [36], Partial Adversarial Domain Adaptation (**PADA**) [37], (4) open set single-source DA: Open Set Back-Propagation (**OSBP**) [39], (5) universal single-source DA: Universal Adaptation Network (**UAN**) [9], (6) closed set multi-source DA: Multisource Domain Adversarial Networks (**MDAN**) [42], Multi-source Distilling Domain Adaptation (**MDDA**) [43], (7) closed set multi-source DA with category shift: Deep CockTail Network (**DCTN**) [41]. These methods are state of the art in their respective settings. In the following experiments, we evaluation all these methods in the UMDA setting.

Evaluation Standards. We evaluate these domain adaptation methods under four standards. (1) **Source-only**: train on the source domains and directly test on the target domain. (2) **Single-best UDA**: train on each source domain and adapt to target domain, in the source shared common label sets $\mathcal{C}_i \cap \mathcal{C}_j$, take the highest accuracy adapted from the i -th and j -th source domain, in the source specific common label sets $\mathcal{C}_j \setminus (\mathcal{C}_i \cap \mathcal{C}_j)$, take the accuracy adapted from the j -th source domain. (3) **Source-combined UDA**: combine all the source domains as a new source domain, train on the new source domain and adapt to target domain. (3) **UMDA**: train on multiple source domains and adapt to target domain, here domain discrepancy and label discrepancy are present between every two domains.

Evaluation Protocols. All the samples with their labels in $\bar{\mathcal{C}}_t$ are viewed as one unified "unknown" class and the final accuracy is averaged by per-class accuracy for $|\mathcal{C}| + 1$ classes. At the testing stage, when the maximum probability of the prediction $\max_{c \in \mathcal{C}_s} G^c(F(\mathbf{x}))$ is less than w_0 , the input image is classified as "unknown", otherwise the input image is classified as $y = \arg \max_{c \in \mathcal{C}_s} G^c(F(\mathbf{x}))$.

Implementation Details. Implementation is in PyTorch and ResNet-50 [66] is used as fine-tuned model, which is pre-trained on ImageNet.

Hyperparameters. We adjust the threshold w_0 on $DW \rightarrow A$. As shown in Table II, we observe that UMAN is not sensitive to w_0 and $w_0 = 0.5$ is always employed in all experiments.

TABLE II: The effect of w_0 on the test accuracy (%) for $DW \rightarrow A$.

w_0						
0.2	0.3	0.4	0.5	0.6	0.7	0.8
90.66	91.65	91.58	90.45	90.19	89.75	88.74

B. Classification Results

We evaluate UMAN and the above methods in various UMDA settings as shown in Table I. The classification results are shown in Table III, IV, V, VI, VII and VIII. Most non-universal methods have negative effects on domain adaptation,

TABLE III: Comparison with the state-of-the-art DA methods of universal multi-source domain adaptation tasks on **Office-31** ($M = 2$, $\xi_1 = \xi_2 = 0.30$ and $\xi_{12} = 0.40$) dataset (Backbone: ResNet-50) measured by classification accuracy (%).

Standards	Methods	Office-31			Avg
	Source	DW	AW	AD	
	Target	A	D	W	
Source-only	Combined	83.28	88.64	83.78	85.23
	Single-best	80.64	87.77	85.50	84.64
Single-best UDA	DANN [15]	80.92	86.45	80.85	82.74
	RTN [18]	80.67	87.04	87.17	84.96
	IWAN [36]	85.64	88.28	88.64	87.52
	PADA [37]	74.42	88.14	83.54	82.03
	OSBP [39]	56.54	81.81	71.34	69.90
	UAN [9]	85.35	94.54	92.03	90.65
Source-combined UDA	DANN [15]	83.43	81.36	84.22	83.00
	RTN [18]	86.70	88.64	83.22	86.19
	IWAN [36]	85.64	87.18	82.31	85.04
	PADA [37]	88.15	89.19	86.09	87.81
	OSBP [39]	57.76	81.54	78.48	72.59
	UAN [9]	82.97	88.64	81.23	84.28
UMDA	DCTN [41]	88.84	89.18	83.73	87.25
	MDAN [42]	85.82	92.82	88.43	89.02
	MDDA [43]	85.40	88.50	82.40	85.43
	UMAN (ours)	90.45	95.12	92.61	92.73

performing worse than no adaptation. Even universal DA method (UAN) suffers from the degradation in performance as the number of source domains increases due to the lack of the consideration of the discrepancy between source domains. The proposed UMAN achieves the best performance and outperforms compared methods by large margins in both source-combined UDA and UMDA settings. This means the proposed UMAN accurately learns useful knowledge across different source domains and promotes the adaptation between source and target domains in their common label set.

To explore the transferability criterion in UAN and UMAN, we plot the Probability Density Distribution (**PDD**) of w^s and w^t in Fig. 6. Compared to PDDs in Fig. 6(a) and 6(b), the PDDs in the source shared and private label sets are harder to be distinguished in Fig. 6(c). This indicates that the transferability criterion of UAN is broken by the distribution discrepancy of same classes in the combined source domain, which assumes that the samples drawn from the same class come from the same distribution. While the PDDs in the proposed UMAN have been separated ideally as shown in Fig. 6(d). Hence, UMAN can mitigate the distribution discrepancy not only between each source domain and target domain, but also between any two distinct source domains.

C. Analysis of UMAN Settings

In this section, we compared the proposed UMAN with methods that achieve the best performance in universal single-source DA and closed set multi-source DA setting, i.e. UAN and MDDA respectively. We discuss UMAN settings from two aspects: (1) the number of source domains and (2) the relationship between label sets.

1) The Number of Source Domains

To analyze the impact of the number of source domains on UMDA, we fix the label set of all the source and target domains and use different number of source domains on each dataset. For (1) $D \rightarrow A$ and $DW \rightarrow A$ (Office-31), fix $|\mathcal{C}_i| = |\mathcal{C}| = 10$, $|\bar{\mathcal{C}}_{s_i}| = |\bar{\mathcal{C}}_s| = 10$, $|\bar{\mathcal{C}}_t| = 11$;

TABLE IV: Comparison with the state-of-the-art DA methods of universal multi-source domain adaptation tasks on **Office-Home** ($M = 2$, $\xi_1 = \xi_2 = 0.12$ and $\xi_{12} = 0.40$) dataset (Backbone: ResNet-50) measured by classification accuracy (%).

Standards	Methods		Office-Home ($M = 2$)												Avg
	Source	Target	CIPr	CIrW	PrRw	ArPr	ArRw	PrRw	ArCI	ArRw	CIrW	ArCI	ArPr	CIPr	
			Ar	Ar	Ar	CI	CI	CI	Pr	Pr	Pr	Rw	Rw	Rw	
Source-only	Combined		70.06	73.04	77.82	58.09	60.20	59.23	77.23	79.82	75.50	85.53	86.79	80.48	73.65
	Single-best		72.56	76.03	77.19	58.45	59.33	58.34	74.91	77.99	76.35	85.73	87.06	84.75	74.06
Single-best UDA	DANN [15]		69.55	76.19	76.56	56.64	56.93	57.13	79.22	80.68	76.80	85.94	86.55	85.19	73.95
	RTN [18]		67.04	74.98	75.80	48.89	54.02	52.45	76.48	78.49	77.17	86.35	86.48	85.37	71.96
	IWAN [36]		73.59	75.41	76.70	55.90	57.52	58.95	78.28	80.65	76.53	86.14	86.08	85.22	74.25
	PADA [37]		58.32	71.61	67.68	38.44	43.02	41.89	68.78	75.48	74.89	77.11	78.60	78.96	64.57
	OSBP [39]		60.94	67.18	67.91	46.78	52.79	51.82	61.38	70.90	71.10	76.05	79.55	77.82	65.35
	UAN [9]		77.82	81.42	81.83	61.68	63.12	61.80	81.59	81.81	79.21	87.10	87.54	86.37	77.61
Source-combined UDA	DANN [15]		71.26	72.75	76.77	56.62	59.57	57.67	80.39	83.04	81.87	86.93	88.39	85.89	75.10
	RTN [18]		71.63	76.48	80.03	55.79	55.36	54.51	80.53	79.87	80.94	86.92	87.47	80.53	74.17
	IWAN [36]		70.02	71.45	74.78	52.96	55.33	51.27	71.73	82.12	73.91	85.62	87.77	84.37	71.78
	PADA [37]		71.55	72.25	76.78	55.06	59.39	54.09	78.28	79.90	73.81	85.64	88.51	83.00	73.19
	OSBP [39]		58.37	66.09	65.92	47.39	53.90	52.38	64.26	68.12	62.80	80.13	80.76	73.48	64.47
	UAN [9]		75.58	77.83	80.66	59.13	62.53	62.01	80.94	83.63	82.60	87.23	87.89	85.85	77.16
UMDA	DCTN [41]		70.60	70.42	67.73	55.53	56.33	48.17	75.26	74.07	68.88	79.71	84.85	82.32	69.49
	MDAN [42]		72.29	71.98	76.09	58.19	62.59	58.35	78.54	80.84	75.58	87.18	88.08	85.09	74.57
	MDDA [43]		68.30	69.89	73.48	51.79	58.30	53.97	76.68	79.01	75.19	84.69	87.03	81.26	71.63
	UMAN (ours)		82.93	83.03	82.23	60.58	61.95	62.06	84.27	84.71	84.73	88.67	90.29	87.80	79.44

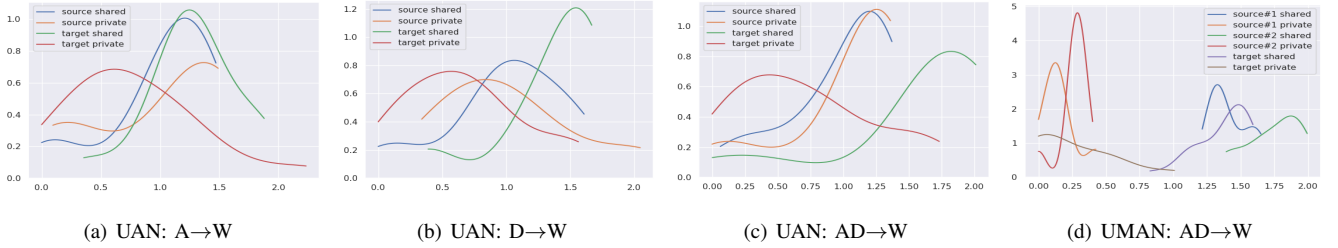


Fig. 6: Probability Density Distribution (PDD) of w^s on (1) 'source shared (#)': source samples in \mathcal{C} or \mathcal{C}_i in 6(d); (2) 'source private (#)': source samples in $\bar{\mathcal{C}}_s$ or $\bar{\mathcal{C}}_{s_i}$ in 6(d); and w^t on (3) 'target shared': target samples in \mathcal{C} ; (4) 'target private': target samples in $\bar{\mathcal{C}}_t$. Note that the source domain in 6(c) is the combination of A and D.

TABLE V: Comparison with the state-of-the-art DA methods of universal multi-source domain adaptation tasks on **Office-Home** ($M = 3$, $\xi_1 = \xi_2 = \xi_3 = 0.08$, $\xi_{12} = 0.00$ and $\xi_{23} = 0.33$) dataset (Backbone: ResNet-50) measured by classification accuracy (%).

Standards	Methods	Office-Home ($M = 3$)					Avg
	Source	CIPrRw	ArPrRw	ArCIrW	ArCIPr		
	Target	Ar	CI	Pr	Rw		
Source-only	Combined	65.36	57.87	79.99	83.24	71.62	
	Single-best	74.55	58.70	76.29	85.75	73.82	
Single-best UDA	DANN [15]	73.34	56.81	78.67	85.82	73.66	
	RTN [18]	71.57	51.45	77.32	85.97	71.58	
	IWAN [36]	74.63	56.82	78.32	85.71	73.87	
	PADA [37]	65.08	40.79	72.41	77.96	64.06	
	OSBP [39]	64.51	49.98	66.82	77.30	67.06	
	UAN [9]	79.88	62.19	80.64	86.93	77.41	
Source-combined UDA	DANN [15]	68.97	53.37	79.70	82.09	71.03	
	RTN [18]	68.72	59.97	77.04	86.00	72.93	
	IWAN [36]	62.01	48.47	77.95	82.33	67.69	
	PADA [37]	62.17	50.87	73.66	81.67	67.10	
	OSBP [39]	44.17	45.98	63.37	68.56	55.52	
	UAN [9]	69.27	60.32	79.78	82.82	73.05	
UMDA	DCTN [41]	64.77	42.09	65.25	70.11	60.56	
	MDAN [42]	67.56	55.36	79.20	86.02	72.04	
	MDDA [43]	44.66	34.54	54.93	53.24	46.84	
	UMAN	79.00	64.68	81.12	87.08	77.97	

For (2) $CI \rightarrow Ar$, $CIPr \rightarrow Ar$ and $CIPrRw \rightarrow Ar$ (Office-Home), fix $|\mathcal{C}_i| = |\mathcal{C}| = 10$, $|\bar{\mathcal{C}}_{s_i}| = |\bar{\mathcal{C}}_s| = 5$, $|\bar{\mathcal{C}}_t| = 50$; For (3) $C \rightarrow R$, $CI \rightarrow R$, $CIPr \rightarrow R$ and $SCIP \rightarrow R$ (VisDA2017+ImageCLEF-DA), fix $|\mathcal{C}_i| = |\mathcal{C}| = 7$, $|\bar{\mathcal{C}}_{s_i}| = |\bar{\mathcal{C}}_s| = 3$, $|\bar{\mathcal{C}}_t| = 2$. We show the transfer gains,

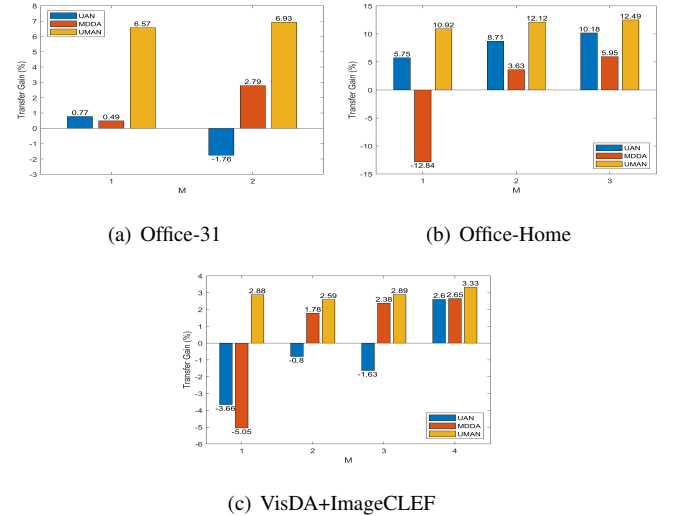


Fig. 7: Transfer gain of UAN (left), MDDA (middle) and UMAN (right) with respect to M on different datasets. Note that negative gain means the accuracy less than that of no transfer.

which are compared to no adaptation in the source-combined setting, on three best methods in Fig. 7. Generally, UAN (the best universal single-source DA method) suffers from negative transfer in some universal multi-source DA settings, and

TABLE VI: Comparison with the state-of-the-art DA methods of universal multi-source domain adaptation tasks on **VisDA2017+ImageCLEF-DA** ($M = 2$, $\xi_1 = \xi_2 = 0.36$ and $\xi_{12} = 0.14$) dataset (Backbone: ResNet-50) measured by classification accuracy (%). (**Com.**: source-combined. **Sin.**: single-best.)

\mathcal{D}_{s_i}	\mathcal{D}_t	Source-only		Single-best UDA						Source-combined UDA						UMDA			
		Com.	Sin.	DANN	RTN	IWAN	PADA	OSBP	UAN	DANN	RTN	IWAN	PADA	OSBP	UAN	DCTN	MDAN	MDDA	UMAN
RC	S	71.28	63.41	64.55	65.35	67.87	66.43	58.61	64.85	76.12	64.56	61.15	74.87	62.42	75.93	62.35	57.73	56.41	76.07
RI	S	71.28	68.14	69.55	72.48	71.64	70.89	67.31	69.05	77.43	77.50	61.11	77.09	68.98	76.44	74.18	62.50	59.75	77.99
RP	S	67.03	69.40	71.02	71.47	70.31	70.74	66.72	70.91	76.52	62.37	73.63	72.51	64.43	76.43	65.25	60.93	58.33	76.65
CI	S	68.24	60.08	62.74	65.90	62.60	64.75	54.62	62.40	64.00	60.25	60.42	69.01	52.42	69.02	67.85	65.30	58.25	69.19
CP	S	61.25	61.76	64.67	64.73	60.83	64.55	53.83	64.87	70.24	72.39	55.51	69.91	47.29	70.40	56.51	58.88	53.94	76.98
IP	S	65.15	66.49	69.47	72.02	65.05	69.07	62.73	69.07	77.41	78.01	60.43	72.83	60.19	76.33	63.11	62.64	55.98	69.56
SC	R	61.10	64.78	67.47	67.09	57.79	66.89	49.15	67.89	69.75	64.63	58.41	60.78	40.20	65.38	67.84	63.03	37.81	74.06
SI	R	61.95	67.20	67.08	67.53	65.52	66.68	52.73	68.05	70.95	63.63	55.27	63.46	41.80	71.81	67.25	59.98	32.23	74.97
SP	R	57.41	67.32	67.51	68.97	61.20	67.04	55.40	68.35	65.48	65.32	54.09	54.96	35.12	61.80	66.16	56.26	36.46	73.46
CI	R	69.32	67.30	67.05	66.74	62.17	66.59	55.34	68.08	74.13	74.67	67.35	65.81	48.05	72.98	62.32	66.06	53.27	76.66
CP	R	61.39	67.42	67.49	68.27	57.85	66.98	58.02	68.72	65.56	62.86	61.20	57.47	39.49	66.32	63.80	60.79	50.57	72.87
IP	R	67.76	69.24	67.10	68.71	65.56	66.77	60.70	68.50	72.66	73.98	69.99	64.00	56.57	69.48	58.84	64.53	55.53	74.16
SR	C	70.77	75.86	78.80	70.44	70.61	81.56	80.29	79.71	64.41	73.71	70.04	74.94	54.57	72.57	78.61	72.74	68.29	81.00
SI	C	69.55	74.43	78.51	70.33	70.33	80.24	80.23	80.91	72.00	70.53	70.29	74.94	57.14	78.00	80.57	72.00	64.00	85.25
SP	C	63.68	72.37	78.69	70.84	70.79	80.19	79.31	80.29	71.51	70.77	70.04	66.37	53.43	66.25	78.37	65.14	66.29	75.75
RI	C	76.41	80.83	79.79	79.31	79.49	82.41	83.16	82.80	79.11	82.29	81.80	80.32	82.00	80.50	81.31	77.14	80.29	87.83
RP	C	71.75	79.29	79.91	79.80	79.87	82.37	82.47	82.17	74.20	80.82	80.82	76.17	67.14	75.75	81.31	74.69	73.96	83.67
IP	C	78.12	77.86	79.67	79.71	79.66	81.06	82.41	83.23	81.06	82.77	81.80	80.57	81.14	82.25	81.06	76.17	84.86	86.33
SR	I	67.59	79.09	79.14	76.33	77.47	79.46	76.44	79.17	73.47	77.14	77.43	72.49	52.29	76.50	73.47	70.04	60.86	81.08
SC	I	72.98	76.11	76.97	75.31	74.94	77.33	68.76	78.83	75.18	76.57	74.57	75.43	54.00	77.50	75.43	73.71	67.14	79.83
SP	I	61.71	78.80	77.44	75.87	76.79	78.20	76.96	80.60	69.80	63.43	61.96	66.61	47.71	73.00	74.94	63.68	62.86	71.42
RC	I	75.92	77.20	78.11	75.94	76.31	78.99	74.30	79.94	76.41	78.61	77.14	76.65	72.00	78.75	74.45	72.25	77.43	85.67
RP	I	72.98	79.69	78.59	76.46	77.99	79.76	81.11	81.63	69.06	76.41	75.92	71.02	58.86	72.50	74.94	73.23	78.00	84.08
CP	I	63.92	76.91	76.23	75.49	75.63	77.73	74.81	81.37	69.06	72.25	72.00	67.35	54.00	69.25	73.71	65.63	74.29	81.42
SR	P	61.23	70.59	70.34	69.16	68.20	70.70	67.53	70.76	60.25	65.71	67.43	61.71	41.43	64.00	65.39	61.23	57.71	71.33
SC	P	61.96	68.70	68.33	65.14	63.66	68.13	58.31	68.81	58.53	66.00	64.57	57.55	35.71	65.25	64.41	60.74	45.71	68.83
SI	P	61.47	68.36	68.17	67.04	65.91	68.30	64.33	68.76	63.18	67.43	67.71	57.80	39.71	65.00	64.17	60.25	54.29	68.83
RC	P	64.17	71.41	72.79	68.00	66.06	71.47	66.54	72.04	66.86	66.86	66.86	66.37	57.43	67.00	63.43	60.49	71.71	72.05
RI	P	66.12	70.77	72.14	69.71	68.29	71.60	71.30	72.00	66.37	66.86	68.08	66.37	64.00	68.25	65.63	61.96	67.43	73.33
CI	P	66.12	69.46	69.46	65.89	63.77	69.07	63.34	70.06	67.11	67.83	68.57	66.86	55.14	69.50	66.86	65.14	68.57	71.42
Avg		66.99	71.39	72.29	71.00	69.14	72.87	67.56	73.46	70.59	70.87	67.85	68.74	54.82	71.80	69.78	65.50	61.07	76.72

MDDA (the best closed set multi-source DA method) suffers from negative transfer in most universal single-source DA settings. The proposed UMAN outperforms the best methods in their specific DA scenarios and keeps a high transfer gain with all the UMDA settings. Meanwhile, we observe that the transfer gain of the proposed UMAN increases as the number of source domains increases. This indicates that learning across more source domains can encourage the transfer of more knowledge to the target domain.

2) The Relationship between Label Sets

To analyze the impact of the relationship between label sets on UMDA, we fix the number of source domains $M = 2$ and select DW \rightarrow A task in Office-31, where all the 31 classes are used.

Impact of the size of the common label set. Let $|\mathcal{C}_{s_1} \cap \mathcal{C}_{s_2}| = 0$, $|\bar{\mathcal{C}}_{s_1}| = |\bar{\mathcal{C}}_{s_2}| = |\bar{\mathcal{C}}_t| - (|\bar{\mathcal{C}}_t| \bmod 3)$, vary $|\mathcal{C}_1|$ and $|\mathcal{C}_2|$ from 0 to 31. Note that $|\mathcal{C}_1| + |\mathcal{C}_2| \leq 31$. As shown in Fig. 8(a), the performance of UAN collapse at $(\mathcal{C}_1, \mathcal{C}_2) = (0, 25), (25, 0)$ with its default hyperparameters. In other combinations of \mathcal{C}_1 and \mathcal{C}_2 , the accuracy of UAN is stable at about 70% and the mean accuracy of UAN is 60.46%. As shown in Fig. 8(b), the performance of MDDA collapse at $(\mathcal{C}_1, \mathcal{C}_2) = (0, 0), (0, 25)$ with its default hyperparameters. The accuracy of MDDA varies widely with the change of $|\mathcal{C}_1|$ and $|\mathcal{C}_2|$ and the mean accuracy of MDDA is 49.40%. In Fig. 8(c), UMAN shows the more stable performance compared with UAN and MDDA, the mean accuracy of UMAN is 70.83% and the accuracy vary from 80% to 90%. In conclusion, the size of the common label set has great influence on UMDA, especially

when the common label sets for distinct source domains differ greatly.

Impact of the size of target private label set. Let $|\mathcal{C}_1| = |\mathcal{C}_2| = 5$, $|\mathcal{C}| = 10$, $|\mathcal{C}_{s_1} \cap \mathcal{C}_{s_2}| = 0$ and $|\bar{\mathcal{C}}_{s_1}| = |\bar{\mathcal{C}}_{s_2}| - (|\bar{\mathcal{C}}_{s_2}| \bmod 2)$, vary $|\bar{\mathcal{C}}_t|$ from 0 to 21. As shown in Fig. 9(a), UAN suffers from negative transfer when $|\bar{\mathcal{C}}_t| < 15$ and MDDA suffers from negative transfer when $|\bar{\mathcal{C}}_t| < 2$. The proposed UMAN improve the adaptation with all size of $\bar{\mathcal{C}}_t$ in UMDA. This indicates that specific universal single-source DA methods and closed set multi-source DA methods are sensitive to the size of target private label set, while UMAN not.

Impact of the size of the intersection of the source common label sets. Let $|\mathcal{C}| = 10$, $|\bar{\mathcal{C}}_{s_1}| = |\bar{\mathcal{C}}_{s_2}| = 5$, $|\mathcal{C}_s| = 20$, $|\bar{\mathcal{C}}_t| = 11$ and vary $|\mathcal{C}_1 \cap \mathcal{C}_2|$ from 0 to 10. For simplicity, we let $|\mathcal{C}_1| = |\mathcal{C}_2| - (|\mathcal{C}_2| \bmod 2)$. As shown in Fig. 9(b), UAN is affected by distribution discrepancy in multiple source domains, and it cannot promote the performance with various sizes of the intersection. MDDA cannot promote the adaptation compared with source-only. While the proposed UMAN accomplishes domain adaptation tasks and improves the performance significantly. Overall, a larger size of the intersection of the source common label sets benefits UMDA.

Impact of the size of the intersection of the source private label sets. Let $|\mathcal{C}_1| = |\mathcal{C}_2| = |\mathcal{C}| = 10$, $|\bar{\mathcal{C}}_s| = 10$ and $|\bar{\mathcal{C}}_t| = 11$, vary $|\bar{\mathcal{C}}_{s_1} \cap \bar{\mathcal{C}}_{s_2}|$ from 0 to 10. For simplicity, we let $|\bar{\mathcal{C}}_{s_1}| = |\bar{\mathcal{C}}_{s_2}| - (|\bar{\mathcal{C}}_{s_2}| \bmod 2)$. As shown in Fig. 9(c), UAN and MDDA cannot promote UMDA, while the proposed UMAN keeps a large transfer gain with varying size of $\bar{\mathcal{C}}_{s_1} \cap \bar{\mathcal{C}}_{s_2}$. In conclusion, the intersection of the source private

TABLE VII: Comparison with the state-of-the-art DA methods of universal multi-source domain adaptation tasks on **VisDA2017+ImageCLEF-DA** ($M = 3$, $\xi_1 = \xi_2 = \xi_3 = 0.30$ and $\xi_{12} = \xi_{23} = 0.20$) dataset (Backbone: ResNet-50) measured by classification accuracy (%). (**Com.**: source-combined. **Sin.**: single-best.)

\mathcal{D}_{s_i}	\mathcal{D}_t	Source-only		Single-best UDA						Source-combined UDA						UMDA			
		Com.	Sin.	DANN	RTN	IWAN	PADA	OSBP	UAN	DANN	RTN	IWAN	PADA	OSBP	UAN	DCTN	MDAN	MDDA	UMAN
RCI	S	58.71	65.37	67.43	67.96	69.06	68.95	63.42	67.03	59.14	66.72	61.28	61.82	54.50	68.28	40.08	52.08	46.59	70.04
RCP	S	59.44	66.99	68.87	67.24	67.74	68.83	62.82	68.89	56.32	63.96	61.25	60.83	47.10	60.42	34.36	49.41	46.15	70.82
RIP	S	69.36	68.57	70.54	72.04	69.44	70.69	65.92	70.29	67.26	68.41	68.56	67.20	52.04	71.06	42.30	57.31	49.42	71.48
CIP	S	66.28	62.92	65.85	67.64	62.97	65.75	57.13	65.66	67.21	67.09	67.26	65.87	52.64	78.42	42.91	60.90	46.62	67.33
SCI	R	57.81	66.63	67.20	67.30	63.31	66.72	52.70	68.02	65.85	60.20	48.59	51.68	43.94	68.24	41.97	56.52	33.59	69.23
SCP	R	54.77	66.72	67.50	68.44	60.07	67.00	54.71	68.24	63.08	60.28	43.00	51.17	37.40	66.54	36.71	56.44	33.15	68.60
SIP	R	64.08	67.93	67.37	68.59	64.45	66.93	56.50	68.32	67.95	67.68	56.63	59.74	45.95	67.79	37.33	61.53	32.64	69.48
CIP	R	67.48	68.00	67.34	68.04	62.22	66.86	58.24	68.34	66.79	70.38	69.10	65.03	55.69	69.85	39.17	65.09	39.80	70.50
SRI	C	72.74	77.16	79.06	73.37	73.50	81.50	81.23	81.24	74.45	69.80	70.29	77.14	59.14	76.41	61.71	75.18	62.29	87.63
SRP	C	66.12	76.13	79.14	73.73	73.77	81.49	80.77	80.77	67.83	68.82	70.04	74.20	50.86	72.74	58.29	71.75	63.43	89.00
SIP	C	69.80	75.06	78.97	73.67	73.63	80.50	80.73	81.53	74.45	69.06	80.57	77.39	57.14	76.17	61.71	72.74	56.29	85.12
RIP	C	76.17	79.44	79.84	79.67	79.76	82.06	82.69	82.79	80.82	82.77	82.53	80.08	70.86	79.35	65.43	74.45	69.14	86.50
SRI	I	70.53	77.56	78.17	75.91	76.36	78.73	73.63	79.34	71.26	76.65	77.39	72.49	57.71	71.51	61.71	73.71	58.00	81.00
SRP	I	68.08	79.21	78.49	76.26	77.47	79.24	78.21	80.59	68.32	72.98	73.47	68.08	53.71	70.04	57.43	76.00	55.71	81.38
SCP	I	70.00	77.97	77.10	75.70	76.23	77.94	74.73	80.41	66.37	72.00	70.00	63.68	50.29	68.32	59.43	69.43	48.57	82.38
RCP	I	66.86	78.79	77.96	76.17	77.26	79.19	78.89	81.19	69.55	72.98	71.02	71.02	60.29	70.53	70.57	75.71	55.43	80.62
SRC	P	60.74	70.51	70.37	67.67	66.17	70.31	64.81	70.70	60.98	65.63	64.89	61.23	45.71	60.98	55.71	66.29	48.29	70.88
SRI	P	63.92	70.34	69.94	68.81	67.66	70.40	67.99	70.67	59.75	66.37	64.89	61.23	49.14	62.45	51.43	67.43	50.57	72.25
SCI	P	58.53	68.93	68.96	66.47	65.17	68.51	62.74	69.21	60.98	70.29	60.00	58.53	43.43	63.18	47.71	66.00	49.14	70.13
RCI	P	64.41	71.14	70.66	68.61	66.97	70.96	68.91	71.53	65.14	66.37	63.43	64.65	64.86	66.12	56.00	68.86	56.86	71.00
Avg		65.29	71.77	72.54	71.16	69.66	73.13	68.34	73.74	66.68	68.92	66.21	65.65	52.62	69.42	51.10	65.84	50.08	75.69

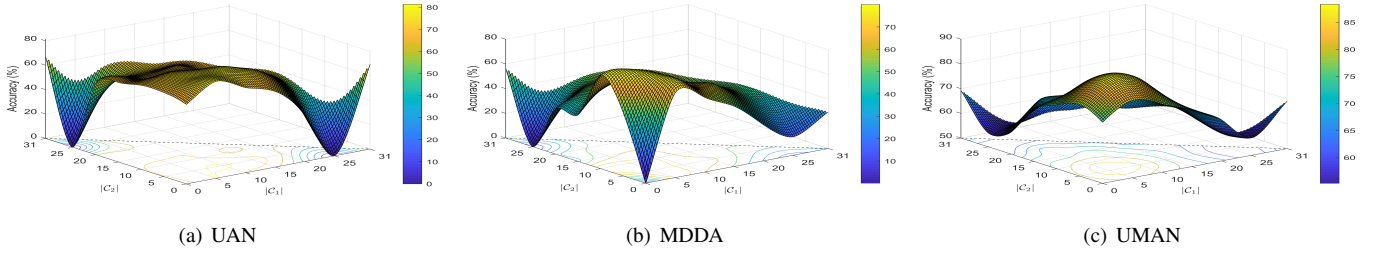


Fig. 8: Accuracy surface with different size of \mathcal{C}_1 and \mathcal{C}_2 on DW \rightarrow A task ($\xi_{12} = 0$).

TABLE VIII: Comparison with the state-of-the-art DA methods of universal multi-source domain adaptation tasks on **VisDA2017+ImageCLEF-DA** ($M = 4$, $\xi_1 = \xi_2 = \xi_3 = 0.22$, $\xi_4 = 0.11$ and $\xi_{12} = \xi_{23} = \xi_{34} = 0.00$) dataset (Backbone: ResNet-50) measured by classification accuracy (%).

Standards	Methods	VisDA2017+ImageCLEF-DA ($M = 4$)					Avg
	Source	RCIP	SCIP	SRIP	SRCP	SRCT	
	Target	S	R	C	I	P	
Source-only	Combined	55.92	53.40	76.50	71.25	60.50	63.51
	Single-best	63.74	66.66	76.29	77.49	69.96	70.83
Single-best UDA	DANN [15]	65.79	67.21	79.03	77.70	69.83	71.91
	RTN [18]	67.66	67.45	73.47	75.80	67.14	70.30
	IWAN [36]	66.05	61.11	73.54	76.19	65.60	68.50
	PADA [37]	67.03	66.75	81.17	78.41	69.71	72.61
	OSBP [39]	59.32	53.37	80.99	73.76	64.01	66.29
	UAN [9]	65.64	68.09	81.09	79.70	70.20	72.94
Source-combined UDA	DANN [15]	57.95	59.93	76.25	64.75	59.75	63.73
	RTN [18]	62.61	57.98	81.50	67.75	62.75	66.52
	IWAN [36]	59.81	41.86	82.25	69.00	64.75	63.53
	PADA [37]	63.09	52.81	76.75	69.25	60.00	64.38
	OSBP [39]	45.41	31.24	49.75	44.50	44.25	43.03
	UAN [9]	56.11	56.80	75.00	67.75	61.00	63.33
UMDA	DCTN [41]	35.15	38.48	66.25	55.75	50.50	49.23
	MDAN [42]	44.11	48.68	68.50	65.25	60.50	57.41
	MDDA [43]	30.88	28.19	60.25	44.50	36.50	40.06
	UMAN	62.95	72.96	88.00	83.25	70.50	75.53

label sets has little effect on UMDA, and no intersection is advocated.

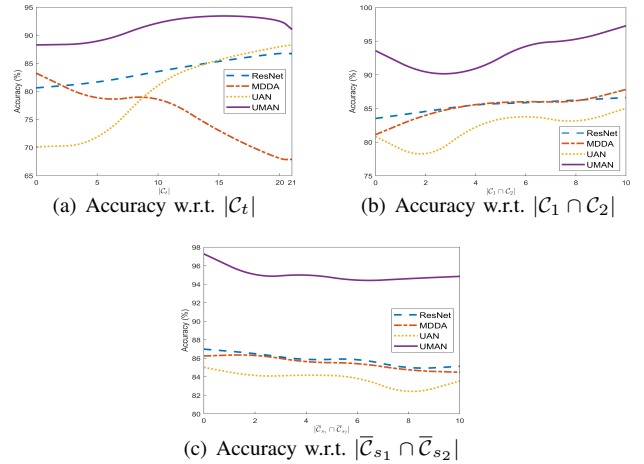


Fig. 9: Accuracy w.r.t. different components of ξ_1 , ξ_2 , ξ_{12} and the threshold on DW \rightarrow A task.

D. Theoretical Verification

In Section III-E, we provide two theorems for UMAN. Here, we implement feature dimensionality reduction and visualization to verify these two theorems. As shown in Fig. 10(a), samples in the common label set of two source domains are aligned and others are separated. This is consistent with

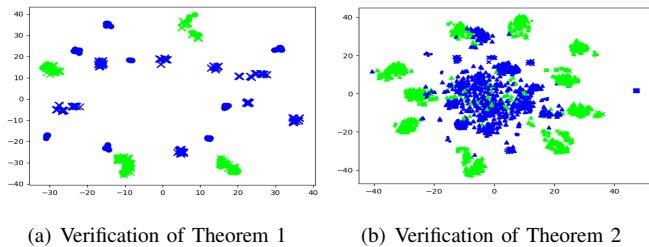


Fig. 10: **t-SNE visualization** on $DW \rightarrow A$ task. In Fig. 10(a), samples come from both D (circle) and W (cross) are colored by their labels: green in their common label set ($C_{s_1} \cap C_{s_2}$) and blue in their private label set. In Fig. 10(b), samples come from both D (circle), W (cross) and A (triangle) are colored by their labels: green in their common label set (C) and blue in their private label set.

Theorem 1. In Fig. 10(b), samples in the common label set of source and target domains are aligned and others are clustered in their private label set. This is consistent with Theorem 2.

V. CONCLUSION

In this paper, we formulated a new domain adaptation setting called universal multi-source domain adaptation (UMDA), where the relationship between each source label set and target label set is unknown. Compared to universal domain adaptation and multi-source domain adaptation, the new challenge in UMDA can be summarized as follows. Firstly, domain discrepancy exists not only between each source domain and target domain, but also between any two distinct source domains. Secondly, as the number of source domains increases, the relationship between label sets of source and target domains becomes more complex. To address these challenges, we proposed a universal multi-source adaptation network (UMAN) with a novel margin vector for UMDA. The margin vector helps adversarial training to better align the multiple source domains and target domain in the common label set, and doesn't incur any increase of model complexity as the number of source domains increases. Moreover, the theoretic guarantees were provided for alignment of distribution of source and target domains in the common label set. Massive experimental results show that UMAN outperforms the state-of-the-art domain adaptation methods by large margins.

ACKNOWLEDGMENTS

This work was supported in part by the National Natural Science Foundation of China under Grant 62071242, 61671252, 61571233 and 61901229; the Natural Science Research of Higher Education Institutions of Jiangsu Province under Grant 19KJB510008.

REFERENCES

- [1] G.-J. Qi, X.-S. Hua, Y. Rui, J. Tang, and H.-J. Zhang, "Two-dimensional multilabel active learning with an efficient online adaptation model for image classification," *IEEE Transactions on Pattern Analysis and Machine Intelligence*, vol. 31, no. 10, pp. 1880–1897, 2008.
- [2] A. J. Joshi, F. Porikli, and N. P. Papanikolopoulos, "Scalable active learning for multiclass image classification," *IEEE transactions on pattern analysis and machine intelligence*, vol. 34, no. 11, pp. 2259–2273, 2012.
- [3] T. Mensink, J. Verbeek, F. Perronnin, and G. Csorba, "Distance-based image classification: Generalizing to new classes at near-zero cost," *IEEE transactions on pattern analysis and machine intelligence*, vol. 35, no. 11, pp. 2624–2637, 2013.
- [4] Z. Akata, F. Perronnin, Z. Harchaoui, and C. Schmid, "Good practice in large-scale learning for image classification," *IEEE Transactions on Pattern Analysis and Machine Intelligence*, vol. 36, no. 3, pp. 507–520, 2013.
- [5] M. Hayat, M. Bennamoun, and S. An, "Deep reconstruction models for image set classification," *IEEE transactions on pattern analysis and machine intelligence*, vol. 37, no. 4, pp. 713–727, 2014.
- [6] Z. Akata, F. Perronnin, Z. Harchaoui, and C. Schmid, "Label-embedding for image classification," *IEEE transactions on pattern analysis and machine intelligence*, vol. 38, no. 7, pp. 1425–1438, 2015.
- [7] Y. Rao, J. Lu, J. Lin, and J. Zhou, "Runtime network routing for efficient image classification," *IEEE transactions on pattern analysis and machine intelligence*, vol. 41, no. 10, pp. 2291–2304, 2018.
- [8] P. P. Busto, A. Iqbal, and J. Gall, "Open set domain adaptation for image and action recognition," *IEEE transactions on pattern analysis and machine intelligence*, 2018.
- [9] K. You, M. Long, Z. Cao, J. Wang, and M. I. Jordan, "Universal domain adaptation," in *Proceedings of the IEEE Conference on Computer Vision and Pattern Recognition*, 2019, pp. 2720–2729.
- [10] O. Lifshitz and L. Wolf, "A sample selection approach for universal domain adaptation," *CoRR*, vol. abs/2001.05071, 2020.
- [11] K. Saito, D. Kim, S. Sclaroff, and K. Saenko, "Universal domain adaptation through self supervision," *CoRR*, vol. abs/2002.07953, 2020.
- [12] J. N. Kundu, N. Venkat, R. V. Babu *et al.*, "Universal source-free domain adaptation," in *Proceedings of the IEEE/CVF Conference on Computer Vision and Pattern Recognition*, 2020, pp. 4544–4553.
- [13] E. Tzeng, J. Hoffman, N. Zhang, K. Saenko, and T. Darrell, "Deep domain confusion: Maximizing for domain invariance," *arXiv preprint arXiv:1412.3474*, 2014.
- [14] M. Long, Y. Cao, J. Wang, and M. Jordan, "Learning transferable features with deep adaptation networks," in *International conference on machine learning*, 2015, pp. 97–105.
- [15] Y. Ganin, E. Ustinova, H. Ajakan, P. Germain, H. Larochelle, F. Laviolette, M. Marchand, and V. Lempitsky, "Domain-adversarial training of neural networks," *The Journal of Machine Learning Research*, vol. 17, no. 1, pp. 2096–2030, 2016.
- [16] P. Haeusser, T. Frerix, A. Mordvintsev, and D. Cremers, "Associative domain adaptation," in *Proceedings of the IEEE International Conference on Computer Vision*, 2017, pp. 2765–2773.
- [17] E. Tzeng, J. Hoffman, T. Darrell, and K. Saenko, "Simultaneous deep transfer across domains and tasks," in *Proceedings of the IEEE International Conference on Computer Vision*, 2015, pp. 4068–4076.
- [18] M. Long, H. Zhu, J. Wang, and M. I. Jordan, "Unsupervised domain adaptation with residual transfer networks," in *Advances in neural information processing systems*, 2016, pp. 136–144.
- [19] E. Tzeng, J. Hoffman, K. Saenko, and T. Darrell, "Adversarial discriminative domain adaptation," in *IEEE Conference on Computer Vision and Pattern Recognition, CVPR*, 2017, pp. 2962–2971.
- [20] K. Saito, K. Watanabe, Y. Ushiku, and T. Harada, "Maximum classifier discrepancy for unsupervised domain adaptation," in *Proceedings of the IEEE Conference on Computer Vision and Pattern Recognition*, 2018, pp. 3723–3732.
- [21] M. Long, Z. Cao, J. Wang, and M. I. Jordan, "Conditional adversarial domain adaptation," in *Advances in Neural Information Processing Systems*, 2018, pp. 1640–1650.
- [22] S. Ben-David, J. Blitzer, K. Crammer, A. Kulesza, F. Pereira, and J. W. Vaughan, "A theory of learning from different domains," *Mach. Learn.*, vol. 79, no. 1–2, pp. 151–175, 2010.
- [23] K. Bousmalis, N. Silberman, D. Dohan, D. Erhan, and D. Krishnan, "Unsupervised pixel-level domain adaptation with generative adversarial networks," in *Proceedings of the IEEE conference on computer vision and pattern recognition*, 2017, pp. 3722–3731.
- [24] S. Sankaranarayanan, Y. Balaji, C. D. Castillo, and R. Chellappa, "Generate to adapt: Aligning domains using generative adversarial networks," in *Proceedings of the IEEE Conference on Computer Vision and Pattern Recognition*, 2018, pp. 8503–8512.
- [25] L. Hu, M. Kan, S. Shan, and X. Chen, "Duplex generative adversarial network for unsupervised domain adaptation," in *Proceedings of the IEEE Conference on Computer Vision and Pattern Recognition*, 2018, pp. 1498–1507.
- [26] Y.-C. Liu, Y.-Y. Yeh, T.-C. Fu, S.-D. Wang, W.-C. Chiu, and Y.-C. Frank Wang, "Detach and adapt: Learning cross-domain disentangled

- deep representation,” in *Proceedings of the IEEE Conference on Computer Vision and Pattern Recognition*, 2018, pp. 8867–8876.
- [27] Z. Murez, S. Kolouri, D. Kriegman, R. Ramamoorthi, and K. Kim, “Image to image translation for domain adaptation,” in *Proceedings of the IEEE Conference on Computer Vision and Pattern Recognition*, 2018, pp. 4500–4509.
- [28] S.-W. Huang, C.-T. Lin, S.-P. Chen, Y.-Y. Wu, P.-H. Hsu, and S.-H. Lai, “Auggan: Cross domain adaptation with gan-based data augmentation,” in *Proceedings of the European Conference on Computer Vision (ECCV)*, 2018, pp. 718–731.
- [29] R. Volpi, P. Morerio, S. Savarese, and V. Murino, “Adversarial feature augmentation for unsupervised domain adaptation,” in *IEEE Conference on Computer Vision and Pattern Recognition, CVPR*, 2018, pp. 5495–5504.
- [30] A. Chadha and Y. Andreopoulos, “Improved techniques for adversarial discriminative domain adaptation,” *IEEE Transactions on Image Processing*, vol. 29, pp. 2622–2637, 2019.
- [31] S. Chen, M. Harandi, X. Jin, and X. Yang, “Domain adaptation by joint distribution invariant projections,” *IEEE Transactions on Image Processing*, vol. 29, pp. 8264–8277, 2020.
- [32] Y. Chen, S. Song, S. Li, and C. Wu, “A graph embedding framework for maximum mean discrepancy-based domain adaptation algorithms,” *IEEE Transactions on Image Processing*, vol. 29, pp. 199–213, 2019.
- [33] R. Li, W. Cao, S. Wu, and H.-S. Wong, “Generating target image-label pairs for unsupervised domain adaptation,” *IEEE Transactions on Image Processing*, vol. 29, pp. 7997–8011, 2020.
- [34] Y. Li, W. Hu, H. Li, H. Dong, B. Zhang, and Q. Tian, “Aligning discriminative and representative features: An unsupervised domain adaptation method for building damage assessment,” *IEEE Transactions on Image Processing*, vol. 29, pp. 6110–6122, 2020.
- [35] Z. Cao, M. Long, J. Wang, and M. I. Jordan, “Partial transfer learning with selective adversarial networks,” in *IEEE Conference on Computer Vision and Pattern Recognition, CVPR*, 2018, pp. 2724–2732.
- [36] J. Zhang, Z. Ding, W. Li, and P. Ogunbona, “Importance weighted adversarial nets for partial domain adaptation,” in *Proceedings of the IEEE Conference on Computer Vision and Pattern Recognition*, 2018, pp. 8156–8164.
- [37] Z. Cao, L. Ma, M. Long, and J. Wang, “Partial adversarial domain adaptation,” in *Proceedings of the European Conference on Computer Vision, ECCV*, 2018, pp. 135–150.
- [38] P. Panareda Busto and J. Gall, “Open set domain adaptation,” in *Proceedings of the IEEE International Conference on Computer Vision*, 2017, pp. 754–763.
- [39] K. Saito, S. Yamamoto, Y. Ushiku, and T. Harada, “Open set domain adaptation by backpropagation,” in *Proceedings of the European Conference on Computer Vision, ECCV*, 2018, pp. 153–168.
- [40] Y. Luo, Z. Wang, Z. Huang, and M. Baktashmotlagh, “Progressive graph learning for open-set domain adaptation,” *arXiv preprint arXiv:2006.12087*, 2020.
- [41] R. Xu, Z. Chen, W. Zuo, J. Yan, and L. Lin, “Deep cocktail network: Multi-source unsupervised domain adaptation with category shift,” in *Proceedings of the IEEE Conference on Computer Vision and Pattern Recognition*, 2018, pp. 3964–3973.
- [42] H. Zhao, S. Zhang, G. Wu, J. M. Moura, J. P. Costeira, and G. J. Gordon, “Adversarial multiple source domain adaptation,” in *Advances in neural information processing systems*, 2018, pp. 8559–8570.
- [43] S. Zhao, G. Wang, S. Zhang, Y. Gu, Y. Li, Z. Song, P. Xu, R. Hu, H. Chai, and K. Keutzer, “Multi-source distilling domain adaptation,” in *Proceedings of the AAAI Conference on Artificial Intelligence*, 2020, pp. 12975–12983.
- [44] S. Zhao, B. Li, X. Yue, P. Xu, and K. Keutzer, “Madan: Multi-source adversarial domain aggregation network for domain adaptation,” *arXiv*, pp. arXiv–2003, 2020.
- [45] K. Li, J. Lu, H. Zuo, and G. Zhang, “Multi-source domain adaptation with distribution fusion and relationship extraction,” in *2020 International Joint Conference on Neural Networks (IJCNN)*. IEEE, 2020, pp. 1–6.
- [46] C. Lin, S. Zhao, L. Meng, and T.-S. Chua, “Multi-source domain adaptation for visual sentiment classification,” in *AAAI*, 2020, pp. 2661–2668.
- [47] Z. Li, Z. Zhao, Y. Guo, H. Shen, and J. Ye, “Mutual learning network for multi-source domain adaptation,” *arXiv preprint arXiv:2003.12944*, 2020.
- [48] X. Peng, Q. Bai, X. Xia, Z. Huang, K. Saenko, and B. Wang, “Moment matching for multi-source domain adaptation,” in *International Conference on Computer Vision, ICCV*, 2019, pp. 1406–1415.
- [49] H. Zhao, S. Zhang, G. Wu, J. P. Costeira, J. M. F. Moura, and G. J. Gordon, “Multiple source domain adaptation with adversarial learning,” in *International Conference on Learning Representations, ICLR*, 2018.
- [50] J. Blitzer, K. Crammer, A. Kulesza, F. Pereira, and J. Wortman, “Learning bounds for domain adaptation,” in *NeurIPS*. Curran Associates, Inc., 2007, pp. 129–136.
- [51] S. Zhao, B. Li, C. Reed, P. Xu, and K. Keutzer, “Multi-source domain adaptation in the deep learning era: A systematic survey,” *CoRR*, vol. abs/2002.12169, 2020.
- [52] Y. Mansour, M. Mohri, and A. Rostamizadeh, “Domain adaptation with multiple sources,” in *NeurIPS*, 2008, pp. 1041–1048.
- [53] J. Hoffman, M. Mohri, and N. Zhang, “Algorithms and theory for multiple-source adaptation,” in *NeurIPS*, 2018, pp. 8256–8266.
- [54] Y. Li, M. Murias, G. Dawson, and D. E. Carlson, “Extracting relationships by multi-domain matching,” in *NeurIPS*, 2018, pp. 6799–6810.
- [55] V. Koltchinskii, D. Panchenko *et al.*, “Empirical margin distributions and bounding the generalization error of combined classifiers,” *The Annals of Statistics*, vol. 30, no. 1, pp. 1–50, 2002.
- [56] Y. Zhang, T. Liu, M. Long, and M. I. Jordan, “Bridging theory and algorithm for domain adaptation,” *arXiv preprint arXiv:1904.05801*, 2019.
- [57] J. Guo, D. J. Shah, and R. Barzilay, “Multi-source domain adaptation with mixture of experts,” *arXiv preprint arXiv:1809.02256*, 2018.
- [58] Y. Zhu, F. Zhuang, and D. Wang, “Aligning domain-specific distribution and classifier for cross-domain classification from multiple sources,” in *Proceedings of the AAAI Conference on Artificial Intelligence*, vol. 33, 2019, pp. 5989–5996.
- [59] S. Rakshit, B. Banerjee, G. Roig, and S. Chaudhuri, “Unsupervised multi-source domain adaptation driven by deep adversarial ensemble learning,” in *German Conference on Pattern Recognition*. Springer, 2019, pp. 485–498.
- [60] X. Peng, Q. Bai, X. Xia, Z. Huang, K. Saenko, and B. Wang, “Moment matching for multi-source domain adaptation,” in *Proceedings of the IEEE International Conference on Computer Vision*, 2019, pp. 1406–1415.
- [61] S. Zhao, G. Wang, S. Zhang, Y. Gu, Y. Li, Z. Song, P. Xu, R. Hu, H. Chai, and K. Keutzer, “Multi-source distilling domain adaptation,” in *Proceedings of the AAAI Conference on Artificial Intelligence*, 2020, pp. 12975–12983.
- [62] K. Saenko, B. Kulis, M. Fritz, and T. Darrell, “Adapting visual category models to new domains,” in *European conference on computer vision*. Springer, 2010, pp. 213–226.
- [63] B. Gong, Y. Shi, F. Sha, and K. Grauman, “Geodesic flow kernel for unsupervised domain adaptation,” in *2012 IEEE Conference on Computer Vision and Pattern Recognition*. IEEE, 2012, pp. 2066–2073.
- [64] H. Venkateswara, J. Eusebio, S. Chakraborty, and S. Panchanathan, “Deep hashing network for unsupervised domain adaptation,” in *Proceedings of the IEEE Conference on Computer Vision and Pattern Recognition*, 2017, pp. 5018–5027.
- [65] X. Peng, B. Usman, N. Kaushik, D. Wang, J. Hoffman, and K. Saenko, “Visda: A synthetic-to-real benchmark for visual domain adaptation,” in *Proceedings of the IEEE Conference on Computer Vision and Pattern Recognition Workshops*, 2018, pp. 2021–2026.
- [66] K. He, X. Zhang, S. Ren, and J. Sun, “Deep residual learning for image recognition,” in *Proceedings of the IEEE conference on computer vision and pattern recognition*, 2016, pp. 770–778.